MNRAS **000**, 1–4 (2016) Preprint 17 August 2016 Compiled using MNRAS LATEX style file v3.0

Chaos in Bar Potential

Anna Juranova;[1] mentors: David N. Spergel,[2] Semyeong Oh[2]
[1]*Department of Theoretical Physics and Astrophysics, Masaryk University, Kotlářská 2, 611 37 Brno, Czech Republic*
[2]*Department of Astrophysical Sciences, Peyton Hall, Princeton University, 4 Ivy Lane, Princeton, NJ USA 08544*

Accepted XXX. Received YYY; in original form ZZZ

ABSTRACT
Amount of chaotic motion in graviational potential caused by presence of a galactic bar is closely related to its parameters. Here we aim at quantifying the fraction of chaotic motion as a function of distance from the galactic center, investigating its dependence on the pattern speed and the total mass of the bar. As a model of the bar we use triaxial Ferrers potential, embedded in a composition of a disk, bulge, and dark matter halo models simulating potential of the Milky Way Galaxy. We classify the nature of stellar orbits using Maximum Lyapunov Exponent (MLE) method of chaos detection on a sample of randomly generated orbits within the bar and its close vicinity.

Key words: galaxies: structure, galaxies: kinematics and dynamics, methods: numerical

1 INTRODUCTION

Large fraction of disc galaxies posses a bar in their central regions. (Buta et al. (2015)) These morphological features are accompanied by chaotic orbits, whose presence is given by a lack of axisymmetry in the gravitational potential caused by bars themselves.(Binney & Tremaine (2008)) Spatial distribution of regions supporting chaotic motion and their properties are closely related to parameters of the potential as shown below.

Studying nature of motion in analytical models can widely contribute to our understanding of potential in our own galaxy. Comparing precise information about position and velocities of stars in inner regions with results from analytical modeling, we can put constraints on form of the potential and its properties. Such information will soon be available from data obtained in GAIA mission.

In this work, we focus on the dependence of distribution of chaotic orbits in the bar potential on its pattern speed and the total mass. We examine sample of 4000 orbits at 20 distances from the center of the potential to its boundaries in aim to classify them as either regular or chaotic.

2 METHODS AND DATA

In this section the model simulating potential of a galaxy is described (Subsect. 2.1) followed by Subsection 2.2 briefly explaining the tool used for distinction between regular and chaotic orbits.

2.1 Analytical model of the potential

For purpose of this work, the bar is represented by a model of Ferrers potential (Ferrers (1877)). Mass density of this triaxial ellipsoid is given by equation:

$$\rho(\vec{x}) = \begin{cases} \rho_c(1-m^2)^2 & \text{if} \quad m < 1, \\ 0 & \text{if} \quad m \geq 1, \end{cases} \tag{1}$$

where $\rho_c = \frac{105}{32\pi}\frac{GM_B}{abc}$ is the central density, M_B is the total mass of the bar and $m^2 = \frac{x^2}{a^2} + \frac{y^2}{a^2b^2} + \frac{z^2}{a^2c^2}$, $a > ab > ac > 0$, with a,ab and ac representing the semi-principal axes of the ellipsoidal bar. Gravitatinal constant G is set to unity. Potential generated by this mass distribution is:

$$V(\vec{x}) = -\frac{105}{96}G^2 M_B \int_\lambda^\infty A^3(\tau)\,\mathrm{d}\tau \tag{2}$$

where

$$A^\nu(\tau) = \frac{\left(1 - \sum_{i=1}^3 \frac{x_i^2}{\tau + a_i^2}\right)^\nu}{[(\tau+a^2)(\tau+a^2b^2)(\tau+a^2c^2)]^{\frac{1}{2}}} \tag{3}$$

is part of an integrand which is used again in following equations. Constants and values of parameters of the bar are set according to the final stage of N-body simulation presented in Machado & Manos (2016). They are listed in Table 1. Lower limit for the integral based on definition of the density distribution is given by relation:

$$\lambda = \begin{cases} \text{unique positive solution of } m^2(\lambda) = 1, & \text{for } m \geq 1 \\ \lambda = 0, & \text{for } m < 1 \end{cases} \tag{4}$$

Table 1. Parameters of the Ferrers bar potential used in the model. Semi-major axis a reaches to 8 kpc, ratios of semi-principal axes lying in y and z axes are set as b and c values respectively. Pattern speed Ω_B and the bar mass M_B vary for different cases we examine and lie in listed intervals.

Parameter	Value
a	8 kpc
b	0.35
c	0.2375
Ω_B	$\langle 10; 27.5\rangle$ km/s/kpc
M_B	$\langle 8.25; 16.5\rangle \times 10^9 M_\odot$

where $m^2(\lambda) = \sum_{i=1}^{3} \frac{x_i^2}{\lambda + a_i^2}$ and $a_1 = a$, $a_2 = ab$, $a_3 = ac$. The analytical expression of the corresponding forces is:

$$F_i = \frac{105}{96} G^2 M_B \frac{bc}{2} \int_\lambda^\infty \frac{x_i}{a_i^2 + \tau} A^2(\tau) \mathrm{d}\tau \tag{5}$$

The bar potential is embedded in a model of Milky Way galaxy's potential provided in *galpy* package written in Python programming languague (Bovy (2015)). The Milky Way model is a composition of Miyamoto-Nagai potential (7) for disk Miyamoto & Nagai (1975), NFW profile (8) for dark matter halo Navarro et al. (1996) and exponentially cut off power-law density profile (6) component for spherical bulge. Parameters of these components are shown in Table 2, further details can be found in Bovy (2015).

$$\rho_b(r) = \rho_0 \left(\frac{r_0}{r}\right)^\alpha \exp - \left(\frac{r}{r_c}\right)^2 \tag{6}$$

$$\Phi_d(R,z) = -\frac{GM_d}{\sqrt{R^2 + (a + \sqrt{z^2 + b^2})^2}} \tag{7}$$

$$\rho_h(r) = \frac{GM_h}{4\pi R_s^3} \frac{1}{(r/R_s)(1 + r/R_s)^2} \tag{8}$$

2.2 Chaos detection method

Various chaos detection methods exist, taking advantage of main differences between regular and chaotic orbits, f.e. frequency diffusion rate described in Price-Whelan et al. (2016) or techniques based on behavior in phase space to be found in Skokos et al. (2007); Skokos & Manos (2014).

Chaos detection method used here belongs to the category mentioned later. The Maximum Lyapunov Exponent (MLE) method is based on a fact that chaotic motion is expressed by exponential divergence of close orbits. Following paragraphs are dedicated to its definition and computation for 3-d.o.f. Hamiltonian function for the motion of a star in a 3 dimensional rotating barred galaxy:

$$H = \frac{1}{2}(p_x^2 + p_y^2 + p_z^2) + V(x,y,z,t) - \Omega_B(xp_y - yp_x). \tag{9}$$

Pattern speed Ω_B is an angular velocity of the bar around z-axis ($\vec{\Omega}_b = \hat{e}_z \Omega_b$), the shortest principal axis, the x direction is along the major axis and the y along the intermediate axis of the bar. The p_x, p_y and p_z are the canonically conjugate momenta, V is the potential, and H is the total energy of the orbit in the rotating frame of reference.

Table 2. Parameters of the Milky Way-like model of potential. Values denoted as f stand for the fraction of radial force in galactic plane at solar radius R_0.

Component	Parameter	Value
	R_0	8 kpc
	$v_c(R_0)$	220 km/s
Bulge	α	−1.8
	r_c	1.9 kpc
	f_b	0.05
	M_b	$5 \times 10^9\, M_\odot$
Disk	a	3.0 kpc
	b	280 pc
	f_d	0.60
	M_d	$6.8 \times 10^{10}\, M_\odot$
Halo	R_s	16 kpc
	$\rho_{DM}(R_0)$	$0.008\, M_\odot \mathrm{pc}^{-3}$
	f_h	0.35 kpc
	M_h	$3.27 \times 10^{11}\, M_\odot$

Equations of motion in this potential are:

$$\begin{aligned}
\dot{x} &= p_x + \Omega_B y, \\
\dot{y} &= p_y - \Omega_B x, \\
\dot{z} &= p_z, \\
\dot{p_x} &= -\frac{\partial V}{\partial x} + \Omega_B p_y, \\
\dot{p_y} &= -\frac{\partial V}{\partial y} - \Omega_B p_x, \\
\dot{p_z} &= -\frac{\partial V}{\partial z}.
\end{aligned} \tag{10}$$

Information about evolution of separation of any two initially infinitesimally close orbits described by deviation vector $\mathbf{w} = (\delta x, \delta y, \delta z, \delta p_x, \delta p_y, \delta p_z)$ needs to be known for the calculation of the MLE. Equations of motion for $\mathbf{w}$ are given by the variational equations:

$$\begin{aligned}
\dot{\delta x} &= \delta p_x + \Omega_B \delta y, \\
\dot{\delta y} &= \delta p_y + \Omega_B \delta x, \\
\dot{\delta z} &= \delta p_z, \\
\dot{\delta p_x} &= -\frac{\partial^2 V}{\partial x \partial x}\delta x - \frac{\partial^2 V}{\partial x \partial y}\delta y - \frac{\partial^2 V}{\partial x \partial z}\delta z + \Omega_B \delta p_y, \\
\dot{\delta p_y} &= -\frac{\partial^2 V}{\partial y \partial x}\delta x - \frac{\partial^2 V}{\partial y \partial y}\delta y - \frac{\partial^2 V}{\partial y \partial z}\delta z - \Omega_B \delta p_x, \\
\dot{\delta p_z} &= -\frac{\partial^2 V}{\partial z \partial x}\delta x - \frac{\partial^2 V}{\partial z \partial y}\delta y - \frac{\partial^2 V}{\partial z \partial z}\delta z.
\end{aligned} \tag{11}$$

In order to compute the value of MLE, both sets of equations (time-dependent set of ordinary differential equations (10) and (11)) need to be solved simultaneously. This requirement arises from the fact that derivatives of the rotating potential depend explicitly on time and (10) are therefore non-autonomous. As described in Binney & Tremaine (2008); Price-Whelan et al. (2016) in further details, the MLE value λ_i is defined as:

$$\lambda_i = \lim_{t \to \infty} \sigma_i(t), \tag{12}$$

where:

$$\sigma_i(t) = \frac{1}{t} \ln \frac{\|\mathbf{w}(t)\|}{\|\mathbf{w}(0)\|}. \tag{13}$$

For obvious practical reasons, it is feasible to use approximation for finite time, the so-called 'finite time MLE' (14), for which $\|\mathbf{w}(0)\|$ and $\|\mathbf{w}(t_i)\|$ are the Euclidean norms of the deviation vector at times $t = 0$ and $t > 0$ respectively.

$$\lambda_N = \frac{1}{t_N} \sum_{i}^{N} \ln \frac{\|\delta\mathbf{w}(t_i)\|}{\|\delta\mathbf{w}_0\|} \tag{14}$$

Examining the evolution of the σ_i in time, we can distinguish between regular and chaotic orbits based on the general trend: for regular motion, the value tends to zero following power law, whereas in the latter case, the value converges to a positive value allowing the deviation vector to increase exponentially.

2.3 Data generation and analysis

To analyze fraction of chaos in our potential, we generated sample of 4000 initial conditions for orbits starting at galactic plane, with uniformly distributed components of velocity vectors. Each subsample constituting of 200 orbits has specific apocentric distance within the bar and is analyzed individually. Orbits are integrated for 20 Gy using leapfrog integrator described in Binney & Tremaine (2008), mainly for sufficient conservation of energy.

Having finite-time MLEs calculated for each sample, the final classification of orbits is based on the final value of MLE. Sufficiently long integration time allowes using reasonably set treshold value to distinguish between each type. For typical example of chaotic orbit the value differs from the one for regular orbit in order of two magnitudes. Validity of this step was confirmed during visual inspection of the descending trend described in 2.2.

3 DISCUSSION

3.1 Dependence on total mass

Chaotic orbits populating sphere at maximal distance being semi-major axis of the ellipsoidal bar was tested for two general cases different in total mass of the bar. Amount of chaos present in

3.2 Dependence on pattern speed

3.3 Figures and tables

Figures and tables should be placed at logical positions in the text. Don't worry about the exact layout, which will be handled by the publishers.

Figures are referred to as e.g. Fig. **??**, and tables as e.g. Table **??**.

4 CONCLUSIONS

The last numbered section should briefly summarise what has been done, and describe the final conclusions which the authors draw from their work.

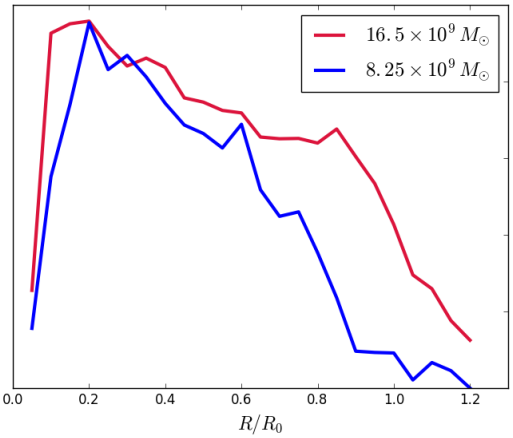

Figure 1. This is an example figure. Captions appear below each figure. Give enough detail for the reader to understand what they're looking at, but leave detailed discussion to the main body of the text.

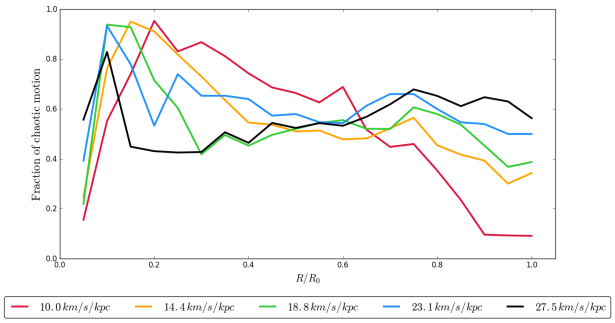

Figure 2. This is an example figure. Captions appear below each figure. Give enough detail for the reader to understand what they're looking at, but leave detailed discussion to the main body of the text.

ACKNOWLEDGEMENTS

The Acknowledgements section is not numbered. Here you can thank helpful colleagues, acknowledge funding agencies, telescopes and facilities used etc. Try to keep it short.

REFERENCES

Binney J., Tremaine S., 2008, Galactic Dynamics, 2nd edn. Princeton University Press
Bovy J., 2015, ApJS, 216, 29
Buta R. J., et al., 2015, The Astrophysical Journal Supplement Series, 217, 32
Ferrers N. M., 1877
Machado R. E. G., Manos T., 2016, MNRAS, 458, 3578
Miyamoto M., Nagai R., 1975, PASJ, 27, 533
Navarro J. F., Frenk C. S., White S. D. M., 1996, ApJ, 462, 563
Price-Whelan A. M., Johnston K. V., Valluri M., Pearson S., Küpper A. H. W., Hogg D. W., 2016, MNRAS, 455, 1079
Skokos C., Manos T., 2014, preprint, (arXiv:1412.7401)

Skokos C., Bountis T. C., Antonopoulos C., 2007, Physica D Nonlinear Phenomena, 231, 30

This paper has been typeset from a TEX/LATEX file prepared by the author.